Rotational Tunnelling of CD_3 Groups in Molecular Crystals as Studied by NMR Spectra

Z. T. Lalowicz*, Ulrike Werner, and W. Müller-Warmuth

Institut für Physikalische Chemie der Westfälischen Wilhelms-Universität, Münster

Z. Naturforsch. **43a**, 219–227 (1988); received January 13, 1988

Tunnelling frequencies of rotating CD_3 groups in solids between about 20 kHz and 2 MHz may be obtained from the ^2H NMR spectra. The theory of the spectral response is developed where quadrupole and dipole–dipole interactions as well as rotational tunnelling are taken into account. Features characteristic of tunnelling, which distinguish the spectra from those of rapidly reorienting deuterated methyl groups, are found from analytically calculated spectra even for the case of very large tunnel splittings. Numerical calculations have been performed for various conditions to determine the tunnel frequency. Experimental spectra measured at 45 MHz and low temperatures have revealed the appearance of rotational tunnelling in CD_3I, CD_3COONa, and $(CD_3COO)_2Cu \cdot H_2O$. In the latter case, a tunnelling frequency of 608 kHz has been extracted from the spectrum at 27 K.

1. Introduction

The rotation of methyl groups in solids between the limits of quantum mechanical tunnelling and classical random reorientation has been extensively studied for many years. The methyl group, having only one rotation axis, provides the simplest example of molecular motion and may be considered as a starting model for more complicated processes. CH_3 tunnelling has been examined in more than 50 different compounds, mainly by inelastic neutron scattering (INS) and nuclear magnetic resonance (NMR) techniques. Tunnel splittings above about 0.5 μeV can be immediately observed by INS, while those below this value are studied by NMR [1]. As far as the latter method is concerned, the analysis of anomalous relaxation rates and level-crossing spectroscopy by field-cycling play the most important role. Only in the exceptional case of highly hindered methyl groups, when the dipolar interaction between the three protons is of the same order of magnitude as the rate of tunnelling, ^1H NMR line shape analysis is of importance. There is a narrow frequency window in which tunnel frequencies may be measured by proton NMR, which has been extended by some innovative techniques up to some hundreds of kHz [2].

The situation changes greatly if we are interested in the isotope effect and in studying the behaviour of CD_3 groups. For nitromethane with its low hindering barrier the tunnel splittings of both CH_3 and CD_3 could be measured by INS, and their ratio was found to be 20 [3]. In most cases, however, CD_3 tunnel splittings are expected to be much smaller, since the barriers are higher, and therefore the ratio of the CH_3 to CD_3 tunnel frequencies should be larger. In the case of NMR, on the other hand, the quadrupole interaction of the deuterons with the electric field gradient becomes the dominant mechanism for both relaxation and shape of the spectra. Spin-lattice relaxation in a system of CD_3 groups was already discussed, and a non-exponentiality was pointed out as an evidence of tunnelling [4]. Rather short spin-lattice relaxation times T_1 prevent the use of the level-crossing method by field-cycling. Analysis of quadrupolar broadened spectra, however, looks quite promising.

The quadrupole coupling constant $e^2 q Q/h$ of the methyl deuterons is of the order of 150–180 kHz [5]. Thus ^2H NMR line shape analysis is expected to give information on tunnel splittings below about 2 MHz. This paper reports the first analysis of spectra from CD_3 groups undergoing tunnelling at low temperatures. We follow the formalism introduced in previous studies of rotational tunnelling effects in ND_4^+ spectra [6–8].

The aim of this research is to supply a convenient method to study rotational tunnelling phenomena of CD_3 groups. We compute the deuteron NMR lineshapes taking into account rotational tunnelling as

* Alexander von Humboldt Foundation Fellow on leave (1985–87) from the Institute of Nuclear Physics, PL-31-342 Kraków, Poland.

Reprint requests to Prof. Dr. W. Müller-Warmuth, Institut für Physikalische Chemie, Universität Münster, Schloßplatz 4–7, D-4400 Münster.

0932-0784 / 88 / 0300-0219 $ 01.30/0. – Please order a reprint rather than making your own copy.

well as quadrupole and dipole–dipole interactions of the deuterons. Chapter 2 gives the theoretical basis for the calculations, while the results of the computations of the spectra are described in Chapter 3 together with the presentation of some powder patterns. Experimental details and results of our first measurements are then discussed in Chapter 4.

2. Basic Theory

2.1. The Hamiltonian

An isolated CD_3 group in a crystal is considered. We are interested in the eigenvalues of the Hamiltonian

$$\hat{H} = \hat{H}_Z + \hat{H}_T + \hat{H}_Q + \hat{H}_D, \tag{1}$$

which consists of Zeeman, tunnelling, quadrupole, and dipole–dipole interaction terms. The Zeeman part describes the interaction between the three deuteron spins (gyromagnetic ratio γ) and the external magnetic field B_0,

$$\hat{H}_Z = -\gamma \hbar B_0 \sum_{i=1}^{3} \hat{I}_z^i = -h \nu_0 M. \tag{2}$$

Concerning the tunnelling Hamiltonian $\hat{H}_T$, in the present treatment we do not require an explicit formula but we will have to consider some general transformation properties.

The quadrupole interaction couples the spin coordinates to the spatial motion. The Hamiltonian may be written as a scalar product of two tensors of the second rank,

$$\hat{H}_Q = h \nu_Q \sum_{i=1}^{3} \sum_{k=-2}^{2} (-1)^k \hat{Q}_k^i V_{-k}^i, \tag{3}$$

where the summation i is extended over the three deuterons. The quadrupole coupling constant is defined as

$$h \nu_Q = \frac{e^2 q Q}{4I(2I-1)} = \frac{1}{4} C_Q,$$

and the dimensionless elements $\hat{Q}_k$ and V_k describe the quadrupole and electric field gradient tensors, respectively. The spatial components V_k must be properly transformed to the laboratory frame of reference by using molecular symmetry arguments.

The quadrupole Hamiltonian (3) may be written in a symmetry adapted form:

$$\begin{aligned}
\hat{H}_Q &= \hat{H}_Q^A + \hat{H}_Q^{E_a} + \hat{H}_Q^{E_b}, \\
H_Q^A &= \frac{1}{12} C_Q \sum_{k=-2}^{2} (\hat{Q}_k^1 + \hat{Q}_k^2 + \hat{Q}_k^3) \\
&\quad \cdot (V_{-k}^1 + V_{-k}^2 + V_{-k}^3), \\
H_Q^{E_a} &= \frac{1}{12} C_Q \sum_{k=-2}^{2} (\hat{Q}_k^1 + \varepsilon \hat{Q}_k^2 + \varepsilon^* \hat{Q}_k^3) \\
&\quad \cdot (V_{-k}^1 + \varepsilon^* V_{-k}^2 + \varepsilon V_{-k}^3), \\
H_Q^{E_b} &= \frac{1}{12} C_Q \sum_{k=-2}^{2} (\hat{Q}_k^1 + \varepsilon^* \hat{Q}_k^2 + \varepsilon \hat{Q}_k^3) \\
&\quad \cdot (V_{-k}^1 + \varepsilon V_{-k}^2 + \varepsilon^* V_{-k}^3),
\end{aligned} \tag{4}$$

with $\varepsilon = \exp\{i \cdot 2\pi/3\}$.

The dipole–dipole interaction between the deuterons of the methyl group is about 500 times smaller than the quadrupole interaction, and only the secular part needs to be considered. This may be expressed in a form analogous to (3):

$$\overline{\hat{H}_D} = C_D \sum_{i<j}^{3} \hat{D}_0^{ij} R_0^{ij}, \tag{5}$$

where $\hat{D}_0^{ij}$ is the spin operator and R_0^{ij} the spatial contribution to the interaction between two deuterons i and j with distance b. The dipolar coupling constant is defined as $C_D = \frac{\mu_0}{4\pi} \gamma^2 \hbar^2 / b^3$.

2.2. Wave Functions

It may be assumed that the methyl group is always in its totally symmetric electronic and vibrational ground state. The essential wave function may then be constructed as a product of rotational wave functions $|G\,R\rangle$ and nuclear spin wave functions $|G\,I\,M\rangle$ with $G = A, E_a, E_b$. Such a product function has to be invariant under a rotation of the methyl group by $2\pi/3$ or $4\pi/3$ or equivalent under even permutations P_j of particles.

Following earlier discussions [9–11], for the CH_3 group the only possible products of rotator and spin functions are $|A\,R\rangle\,|A\,I\,M\rangle$, $|E_a\,R\rangle\,|E_b\,I\,M\rangle$ and $|E_b\,R\rangle\,|E_a\,I\,M\rangle$. In contrast to CH_3 groups, where A symmetry species are necessarily coupled with a total spin of $I = 3/2$ and E species with $I = 1/2$, such correspondence does not exist for CD_3. Here we have 11

A-functions with total spin $I = 3$, 1, and 0, and 16 E symmetry functions with total nuclear spin 2 and 1.

The deuterons of the methyl group may be regarded as the vertices of an equilateral triangle labeled $(a\,b\,c)$. Localization of an apex x in the i-th potential minimum we describe by a function $\Phi_i(x)$. The potential is assumed to have C_3 point symmetry. We may describe three possible space orientations of the triangle by pocket state wave functions

$$\begin{aligned}\Phi_R(E) &= \Phi_1(a)\,\Phi_2(b)\,\Phi_3(c),\\ \Phi_R(C_3) &= \Phi_1(c)\,\Phi_2(a)\,\Phi_3(b),\\ \Phi_R(C_3^2) &= \Phi_1(b)\,\Phi_2(c)\,\Phi_3(a),\end{aligned} \tag{6}$$

which are generated from each other through rotations C_3 and C_3^2.

Symmetry adapted wave functions result from this basis by application of the character table of the CD_3-group:

$$|A\,R\rangle = \frac{1}{\sqrt{3}}[\Phi_R(E) + \Phi_R(C_3) + \Phi_R(C_3^2)], \tag{7}$$

$$|E_a\,R\rangle = \frac{1}{\sqrt{3}}[\Phi_R(E) + \varepsilon\,\Phi_R(C_3) + \varepsilon^*\,\Phi_R(C_3^2)],$$

$$|E_b\,R\rangle = \frac{1}{\sqrt{3}}[\Phi_R(E) + \varepsilon^*\,\Phi_R(C_3) + \varepsilon\,\Phi_R(C_3^2)].$$

Analogously, simple product spin functions $\Phi_I^M(E) = m_1(a)\,m_2(b)\,m_3(c)$ etc. lead to symmetrized spin wave functions. Products of the symmetrized spin and space wave functions are invariant to C_3 symmetry rotations. However, these symmetrized spin wave functions are not eigenfunctions of the total spin I. Therefore we will subsequently use the notation $|G\,M\rangle$.

There are altogether $(2I+1)^3 = 27$ spin wave functions for a system of three deuterons. The first three of A symmetry may be pointed out right away: $|A\,3\rangle = |\alpha\alpha\alpha\rangle$, $|A\,0\rangle = |o\,o\,o\rangle$, $|A-3\rangle = |\beta\beta\beta\rangle$, where α, o, β present the states with $m_i = 1, 0, -1$, respectively. The remaining simple product spin wave functions may also be easily generated.

For numerical calculations it is particularly convenient to set up the matrix representation (1) in a slightly extended basis of the simple product spin basis [12]

$$\psi_i^M = |m_1, m_2, m_3\rangle = \frac{1}{\sqrt{3}}\sum_j \Phi_R(P_j)\,\Phi_I^M(P_j), \tag{8}$$

where summation over all symmetrie operations allows finding all equivalent and practically undistinguishable positions. By this the wave functions establish a connection between spin states and pocket states and are independent of the particular deuteron sites that carry the specific space and rotator wave functions. In this basis we may already look for the expectation values of the tunnelling Hamiltonian.

2.3. Tunnelling Hamiltonian Matrix

The magnitude of the tunnel splitting is given by the overlap of wave functions in different pocket states. Rather than considering explicit expressions for the tunnelling Hamiltonian the following overlap integrals are defined in the basis (6) for the space and spin functions:

$$\begin{aligned}\langle\Phi_R(E)\cdot\Phi_I^M|\hat{H}_T|\,\Phi_R(E)\cdot\Phi_I^M\rangle &= C_0,\\ \langle\Phi_R(E)\cdot\Phi_I^M|\hat{H}_T|\,\Phi_R(C_3)\cdot\Phi_I^M\rangle &= -\Delta,\\ \langle\Phi_R(E)\cdot\Phi_I^M|\hat{H}_T|\,\Phi_R(C_3^2)\cdot\Phi_I^M\rangle &= -\Delta.\end{aligned} \tag{9}$$

For the three simple A functions in representation (8) we obtain, e.g., $\langle\alpha\alpha\alpha|\hat{H}_T|\alpha\alpha\alpha\rangle = C_0 - 2\Delta$. Remaining spin wave functions (8) are organized in sets of three giving 3×3 matrix representations of $\hat{H}_T$. There are always diagonal elements equal to C_0 while all off-diagonal elements equal $-\Delta$. Diagonalization leads to the symmetry adapted $|G\,M\rangle$ wave functions and eigenvalues -2Δ and Δ for A and E states, respectively. Thus the tunnel splitting amounts to $h\nu_t = 3\Delta$ with the A levels lying the lowest in energy.

3. Lineshape Calculations

The major part of these calculations consists of the determination of the eigenvalues of the general Hamiltonian (1). In strong magnetic fields, the matrix of $\hat{H}$ factorizes into quadratic submatrices with dimensions 1×1 (for $M = \pm 3$), 3×3 (for $M = \pm 2$), 6×6 (for $M = \pm 1$), and 7×7 (for $M = 0$). These submatrices may be diagonalized separately. However, for the purpose of calculations of spectra in weak magnetic fields, the whole 27×27 matrix must be diagonalized. In this case the off-diagonal matrix elements $\Delta M = \pm 1$, ± 2 of the quadrupole Hamiltonian (3) cannot be ignored.

The transition frequencies and probabilities are calculated for all possible differences between adjacent eigenstates, and the spectra are obtained from summing up over all allowed transitions with $\Delta M = 1$. Single crystal spectra are calculated for definite orien-

tations of the C_3 axis with respect to B_0. Powder patterns result from spatially weighted sums over all possible orientations where geometric arguments lower the number of necessary orientations. Convolution with a Gaussian function accounts for broadening by intermolecular dipolar interactions.

3.1. High field ^2H NMR Spectra for Large Tunnel Splittings

We assume first that both $\gamma\hbar B_0$ and Δ [cf. (2) and (9)] are much larger than C_Q [cf. (3)]. Then only the secular part of the quadrupole interaction needs to be considered. Dipolar interaction may be neglected completely since $C_D \approx C_Q/500$. In this case we prefer to use the symmetry adapted wave functions $|G\,M\rangle$ as a basis, thus allowing the spectra to be calculated analytically. Zeeman and tunnel splittings determine the zeroth order energy values (see Fig. 1), where the Zeeman-levels are split into a single A-level (displacement -2Δ) and a twofold degenerate E-level ($+\Delta$). The quadrupole interactions lead to small energy shifts and to admixtures within the E-states resulting in additional splittings.

The 27×27 matrix of the general Hamiltonian $\hat{H}$ factorizes into three A type diagonal terms $\pm 3h\nu_0 - 2\Delta + Q_{AA}$ and $-2\Delta + Q_{AA}$, respectively, as well as eight 3×3 submatrices of the general form

$$\begin{pmatrix} -h\nu_0 M - 2\Delta + Q_{AA} & Q_{AE_a} & Q_{AE_b} \\ Q_{E_aA} & -h\nu_0 M + \Delta + Q_{E_aE_a} & Q_{E_aE_b} \\ Q_{E_bA} & Q_{E_bE_a} & -h\nu_0 M + \Delta + Q_{E_bE_a} \end{pmatrix} \tag{10}$$

with $Q_{GG'} = \langle G\,M|\hat{H}_Q|G'\,M\rangle$. For very large Δ we may neglect $Q_{GG'}$ elements between A and E states, and we need to diagonalize only a 2×2 matrix for the E states. From the calculations we obtain the energy eigenvalues and eigenstates.

The quadrupole shifts of the A-levels amount to 0, $\pm\beta$, or 2β, whereas those of the E-levels are equal to $\pm\alpha$, $-\beta$ or $\beta \pm \alpha$, using the abbreviations

$$\alpha \equiv h\nu_Q \sin\theta\sqrt{1+\cos^2\theta - \sqrt{2}\sin 2\theta\cos 3\varphi},$$
$$\beta \equiv 1/2\, h\nu_Q (3\cos^2\theta - 1). \tag{11}$$

The angles θ and φ define an orientation of B_0 in the molecular reference frame. In accordance to the C_3-symmetry, φ appears only with a periodicity of $2/3\,\pi$.

After including transition probabilities the observable transition energies are listed in Table 1.

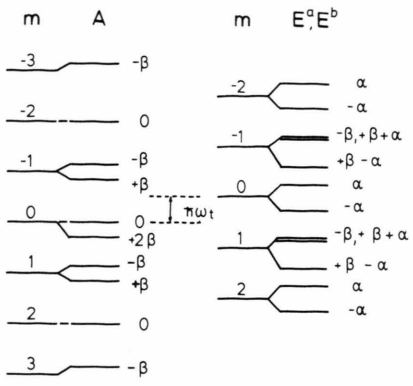

Fig. 1. The energy-level scheme for CD_3 group symmetry species in a high magnetic field ($\theta = 90°$, $\alpha = -2\beta = h\nu_Q$). Only the rotator ground state is shown (not to scale).

Table 1. Components in the ^2H NMR spectra of tunnelling CD_3 groups for $\nu_0 > \nu_t \gg \nu_Q$.

Symmetry component	Transition frequency	Spectral positions for $\theta = 90°$ $\varphi = 0°$	Relative intensity
A	$\nu_0 \pm \beta$	$\pm 1/2\,\nu_Q$	0.76
E	$\nu_0 \pm \beta$	$\pm 1/2\,\nu_Q$	0.24
E	$\nu_0 \pm \beta \pm \alpha$	$\pm 3/2\,\nu_Q$	0.28
E	$\nu_0 \pm \beta \pm 2\alpha$	$\pm 5/2\,\nu_Q$	0.12

For the case $\theta = \pi/2$, $\varphi = 0°$ the Hamiltonian (10) has the following eigenstates (in representation 8):

$$\psi^A = \frac{1}{\sqrt{3}}(\psi_i^M + \psi_j^M + \psi_k^M),$$
$$\psi_1^E = \frac{1}{\sqrt{6}}(-\psi_i^M + 2\psi_j^M + \psi_k^M), \tag{12}$$
$$\psi_2^E = \frac{1}{\sqrt{6}}(\psi_i^M - \psi_k^M),$$

where i, j, k depend on the choosen sequence of basis functions.

The resulting A and E spectra and the total spectrum are shown both for a single crystal (left) and for a powder (right) in Figure 2. The powder pattern is

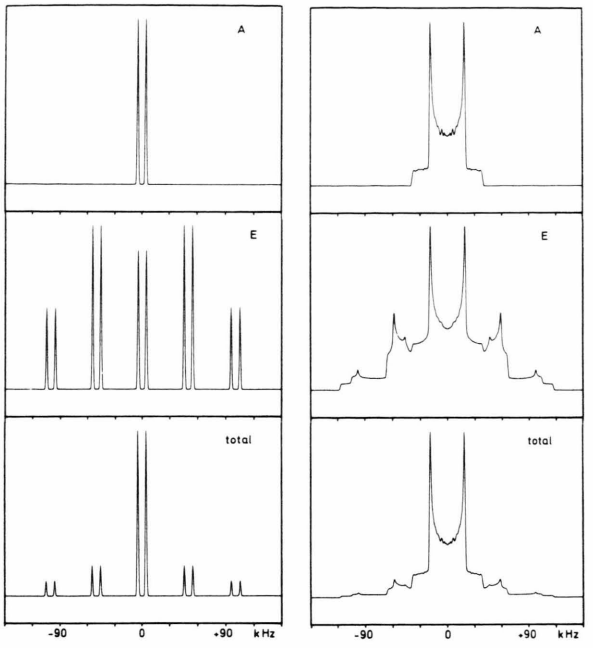

Fig. 2. Representation of the analytically calculated A- and E-symmetry species spectra along with the total spectra for single crystals ($\theta = 120°$, $\varphi = 0°$, left) and crystal powders (right); $C_Q/h = 154.6$ kHz

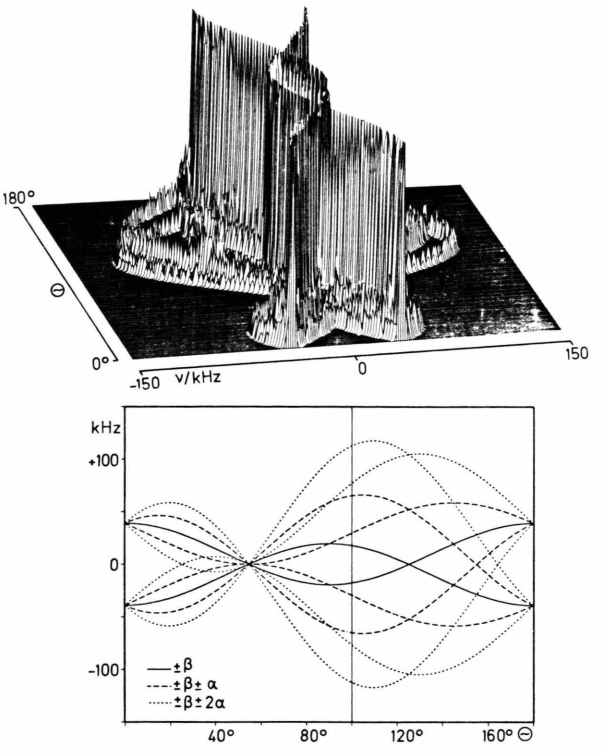

Fig. 3. Angular dependence of single crystal spectra (top) and positions of lines (bottom) for $\nu_t \gg 4\,\nu_Q = 154.6$ kHz and $\varphi = 0$.

composed of a Pake doublet with a frequency separation of ν_Q of the singularities (characteristic of a rapidly reorienting CD_3 group), another Pake doublet with a separation $3\,\nu_Q$ (characteristic of a rigid CD_3 group) and, finally, by a weak pair of peaks separated by $5\,\nu_Q$. Assumption of a motional model of tunnelling with reorientation, simulated by averaging the quantity α over φ, would still give a result different from that of reorientation only.

The angular dependence of the position of the peaks for single crystals is shown in Figure 3.

3.2. High Field Spectra at Tunnelling Frequencies below 2 MHz

The ^2H NMR spectra of CD_3 groups become sensitive to the tunnelling frequency when $\nu_t = 3\,\Delta/h < 2$ MHz. For such cases the spectra had to be calculated numerically. For powder patterns we have to distinguish the two cases $\nu_t > 4\,\nu_Q$ and $\nu_t < 4\,\nu_Q$. The quasi-three-dimensional representation of Fig. 4 summarizes the result. Standard procedures available at the Computer Centre of the University of Münster have been used.

For $\nu_t \gg 4\,\nu_Q$ the results are of course reminiscent of the spectrum of Figure 2. When ν_t is increased, each line of the interior Pake doublet splits into a triplet whose side lines depend sensitively on the tunnelling frequency (Figure 5). The hyperbolic development of the line splitting points to a prescription by perturbation theory which predicts for the energy shift of A-levels

$$\delta E_A = \sum_{E_a, E_b} \frac{(\langle A\,M|\hat{H}_Q|E\,M\rangle)^2}{E_E - E_A} \sim \frac{1}{h\,\nu_t}. \qquad (13)$$

If ν_t approaches $4\,\nu_Q$ (cf. Figs. 4 and 5), the more intense interior side lines coalesce into one. The tunnelling frequency is most easily calculated from the separation of the interior peaks. The positions of the exterior singularities with a separation of about 120 kHz is not very sensitive to tunnelling. This arises from the fact that these peaks result from quadrupolar interactions between E levels which are degenerate for any pure tunnel Hamiltonian.

The most important feature of the spectra for $\nu_t < 4\,\nu_Q$ (Fig. 4, bottom) is the exterior (rigid lattice)

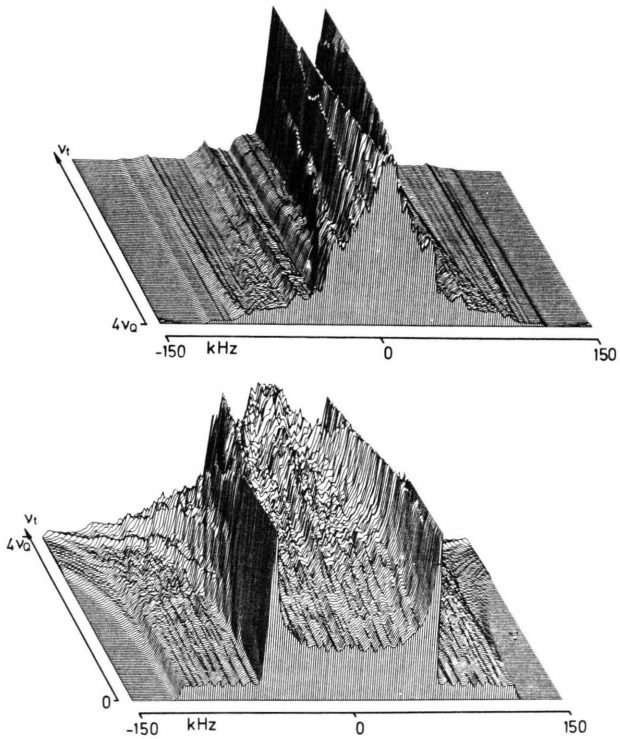

Fig. 4. Representation of the computed powder patterns for $\nu_t > 4\nu_Q = 154.6$ kHz (top) and $\nu_t < 4\nu_Q$ (bottom).

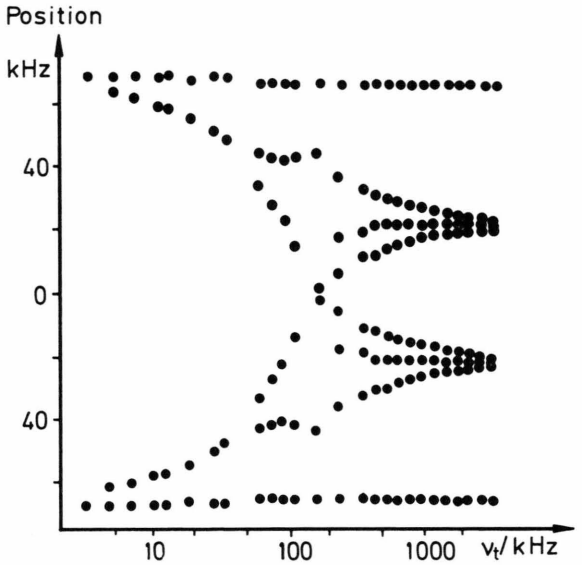

Fig. 5. Position of the inner peaks of the ^2H NMR spectra of Fig. 4 as a function of the tunnelling frequency.

Pake doublet with a separation of the peaks of about 120 kHz. From these lines sidebands split off if ν_t increases from zero towards the value of the quadrupole coupling constant; the position of the inner peaks can be taken from Figure 5. As ν_t approaches $4\nu_Q$ a broad inner part dominates the spectra which becomes higher and sharper.

^2H NMR spectra of single crystals, in principle, show the same behaviour. However, measurements on single crystals would give more precise ν_t values, particularly for 50 kHz $< \nu_t <$ 300 kHz and $\nu_t > 1.5$ MHz. In these ranges the resolution of polycrystalline spectra is not sufficient to allow calculations of ν_t directly.

3.3. Spectra in "Weak" Magnetic Fields

If the Zeeman splitting is no longer very much larger than the tunnel splitting, which may already be the case for $B_0 < 3$ T, the quadrupole interaction may produce an admixture of states with different symmetry of neighbouring Zeeman levels. The spectra then broaden and become asymmetric. Particularly strong effects occur if the level-crossing condition, $\nu_t = \nu_0$ or $\nu_t = 2\nu_Q$, is fulfilled. Figure 6 gives an example of such

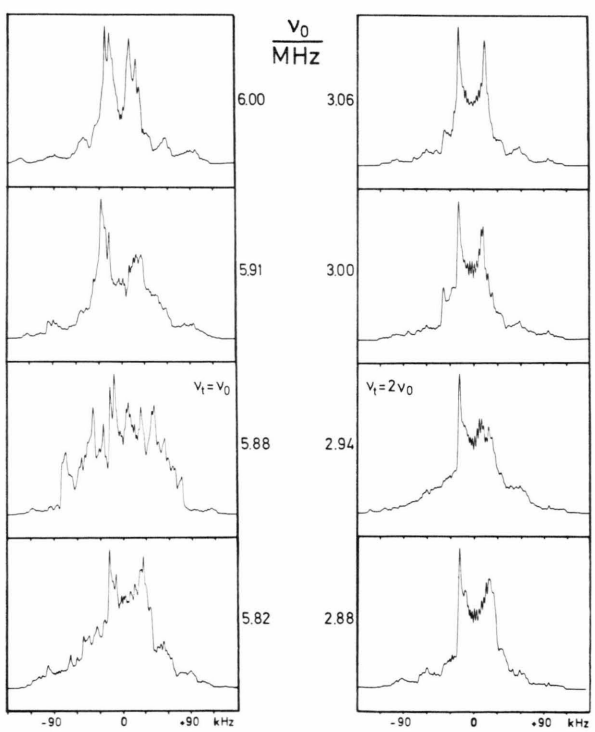

Fig. 6. Calculated powder patterns for resonance frequencies near the level-crossing condition for a CD_3 group tunnelling at $\nu_t = 5.88$ MHz.

a behaviour, which may be used to extend the range of measurable tunnelling frequencies ν_t.

3.4. Influence of a Sixfold Contribution to the Potential

Purely threefold potentials hindering the rotation have been assumed so far. Consideration of a sixfold contribution (mixed V_3, V_6 potential) leads to an additional splitting of both the A and the E-levels. Calculated spectra (Fig. 7) demonstrate that the lineshapes differ from those for a purely threefold potential only if both splittings become of the same order of magnitude. In this case an admixture of states takes place.

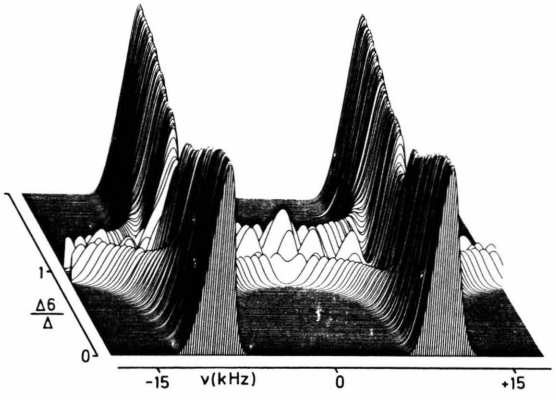

Fig. 7. Computed single crystal spectra for a fixed threefold and an increasing sixfold contribution to the hindering potential. $2\Delta_6$ is the additional splitting of the A-levels, Δ_6 that between E-levels.

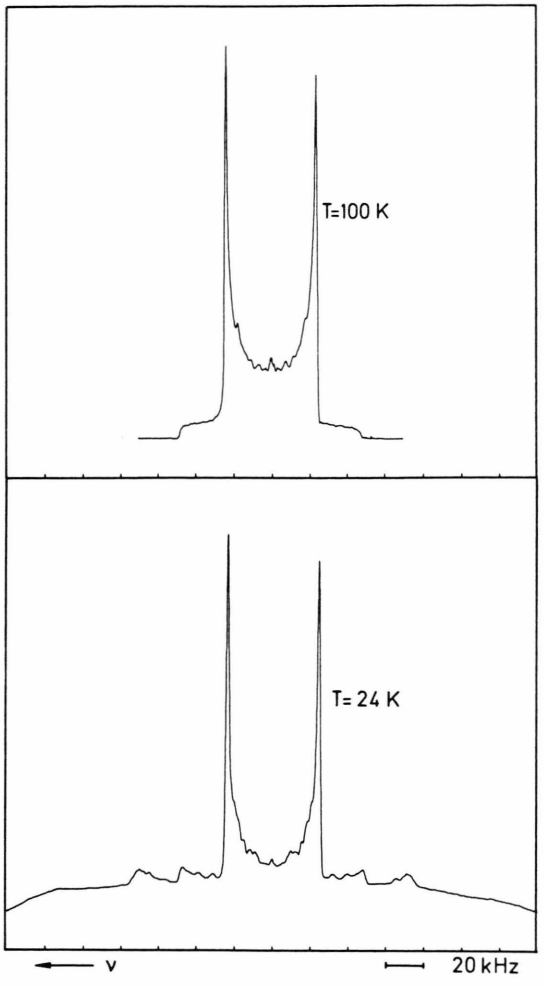

Fig. 8. ^2H NMR spectra of CD_3I at 46.07 MHz measured at two different temperatures.

4. Experimental Results

Measurements of the ^2H NMR spectra were carried out using a Bruker CXP 300 FT-spectrometer. The NMR frequency ν_0 was 46.07 MHz in a magnetic field of 7.047 T. A home-made liquid helium continous flow cryostat was employed, with a two chamber probe head inside. The probe chamber could be evacuated and filled with gaseous helium. Special attention has been paid to finding a compromise between good heat contact and radio-frequency breakthrough. In the low temperature range, short pulses (0.2–0.5 μs) with a repetition time of 50 or 100 ms were used to produce the free induction decay. Despite of a certain distortion the essential features of the spectra could be observed.

Deuterated methyl iodide, CD_3I, and polycrystalline sodium acetate, CD_3COONa were commercially obtained, whereas copper acetate $(CD_3COO)_2Cu \cdot H_2O$ was prepared from copper hydroxide and acetic acid. Oxygen was removed by standard techniques, and the samples were sealed in glass ampoules.

Comparison of the spectra of CD_3I (Fig. 8) at temperatures of 100 K and 24 K discriminates clearly between the lineshape for a rapidly reorienting CD_3 group and the features characteristic of tunnelling as discussed in Chapt. 3.1 and Figure 2. In addition to the peaks of the interior Pake doublet, at 24 K peaks with separation $3\nu_Q$ can be recognized. The measured spectra could be simulated by assuming a very large

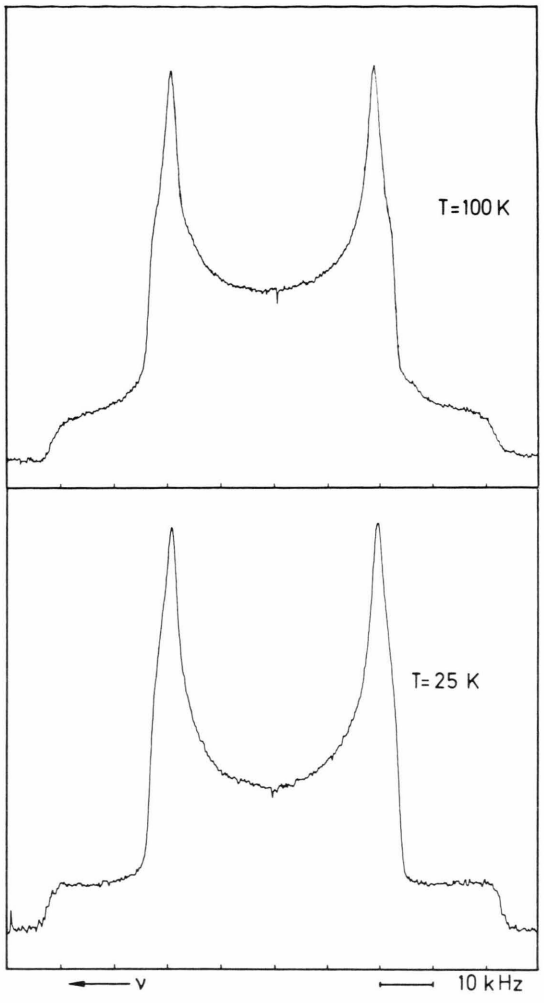

Fig. 9. ^2H NMR spectra of CD_3COONa at 46.07 MHz measured at two different temperatures.

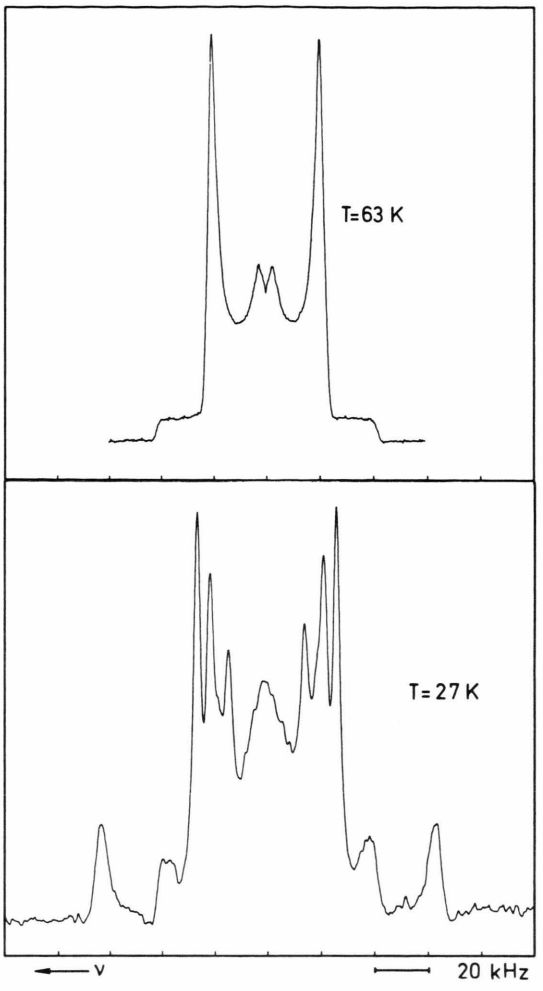

Fig. 10. ^2H NMR spectra of $(CD_3COO)_2Cu \cdot H_2O$ at 46.07 MHz measured at two different temperatures.

Table 2. Experimental results of the tunnelling frequencies ν_t and quadrupole coupling constants C_Q as derived from the spectra. For the purpose of comparison, ν_t values are given for CH_3 tunnelling.

	T / K	ν_t / MHz	C_Q/h / kHz	Ref.
CD_3I	24	>2	187 ± 9	this work
CH_3I	3.7	590	–	[14]
CD_3COONa	25	>2	152 ± 8 172 ± 8	this work
CH_3COONa	46	360	–	[15]
$(CD_3COO)_2Cu \cdot H_2O$	27	0.61 ± 0.06	168 ± 8	this work
$(CH_3COO)_2Cu \cdot H_2O$	4.2	64	–	[16]

tunnel splitting and a quadrupole coupling constant as given in Table 2.

^2H NMR spectra of CD_3COONa (Fig. 9) may be interpreted in terms of non-equivalent CD_3 groups which lead to the occurrence of two quadrupole coupling constants. This interpretation with an asymmetry parameter $\eta = 0$ is not unique but does not contradict the crystal structure [13]. The spectra can be simulated by the model of a rapidly reorienting CD_3 group assuming two different types of distinct rotators with the quadrupole coupling constants of Table 2. Further details characteristic of tunnelling cannot be resolved in the low temperature spectrum,

probably as a consequence of the presence of non-equivalent methyl groups.

The low temperature spectrum of copper acetate, Fig. 10, reveals all of the details necessary for a determination of the tunnelling frequency. As expected from the calculations of Chapt. 3.2, each line of the interior Pake doublet splits into a triplet. The exterior doublet is visible as well. This is an excellent example of a spectrum which shows all of the features of tunnelling with a tunnelling frequency not too much larger than the quadrupole splitting (cf. Table 2). Minor blemishes in the experimental spectrum arise for technical reasons (e.g. no solid echo possible).

Table 2 presents the numerical results and compares the tunnelling frequencies obtained in this work with those known for the protonated species [14–16]. The ratio of the CH_3 to CD_3 tunnel frequencies is about 100 for copper acetate. For methyl iodide and sodium acetate the CD_3 tunnelling frequencies are much larger than 2 MHz.

5. Conclusion

It has been shown theoretically and verified experimentally that the determination of tunnel frequencies of CD_3 groups by ^2H NMR lineshape analysis is possible when $\nu_t < 2$ MHz. Even in the case, where the tunnel splitting is too large to be determined, the spectra of CD_3 groups undergoing tunnelling show features which distinguish them from spectra due to classical rotation at high temperatures.

The features observed in the ^2H NMR spectra of tunnelling CD_3 groups are directly related to the transformation properties of the quadrupole Hamiltonian. This may be understood by analyzing the role of its various matrix elements between the symmetry adapted functions. E_a and E_b states are split due to secular elements of $\hat{H}_Q$. This leads to sidebands which are not present in the spectra narrowed by reorientation at high temperatures. Such mixing terms are absent in the dipole–dipole interaction, and CH_3 spectra present no difference between tunnelling with large ν_t and reorientation [10]. The terms between A and E states provide second order energy corrections, which are inversely proportional to ν_t. These, observed on a background of first order shifts supply means of measuring the tunnelling frequency. However, for resolution reasons this is only possible up to about 2 MHz. The accuracy and range of the determination may be extended using single crystals. In the case of ND_4^+, the A spectral components are narrow and the range of measurable ν_t extends up to about 7 MHz, even for powder samples [8]. Finally, the nonsecular terms in $\hat{H}_Q$ cause a spectral dependence also on the Larmor frequency provided $\nu_0 < 20$ MHz. Asymmetry and broadening of the central doublet components are observed and at level-crossing $\nu_t = \nu_0$ the structure is smeared out completely. It is anticipated that low field measurements may extend the range of measurable tunnelling frequencies up to about 20 MHz.

Acknowledgement

The contribution of the Alexander von Humboldt-Foundation to this research is gratefully acknowledged.

[1] H. Langen, A.-S. Montjoie, W. Müller-Warmuth, and H. Stiller, Z. Naturforsch. **42a,** 1266 (1987) and references therein.
[2] P. J. Mc Donald, G. J. Barker, S. Clough, R. M. Green, and A. J. Horsewill, Molec. Phys. **57,** 901 (1986) and references therein.
[3] B. Alefeld, I. S. Anderson, A. Heidemann, A. Magerl, and S. F. Trevino, J. Chem. Phys. **76,** 2758 (1982).
[4] J. Tang, A. Pines, and S. Emid, J. Chem. Phys. **73,** 172 (1980).
[5] M. Rinné and J. Depireux in Advances in Nuclear Quadrupole Resonance (J. A. S. Smith, Ed.), Vol. 1, p. 357 (1974) Heiden, London.
[6] T. T. Lalowicz and W. Sobol, J. Phys. C: Solid State Phys. **16,** 2351 (1983).
[7] Z. T. Lalowicz, J. Phys. C: Solid State Phys. **16,** 2363 (1983).
[8] L. P. Ingman, E. Koivula, Z. T. Lalowicz, M. Punkkinen, and E. E. Ylinen, J. Chem. Phys., in press.
[9] J. H. Freed, J. Chem. Phys. **43,** 1710 (1965).
[10] F. Apaydin and S. Clough, J. Phys. C: Solid State Phys. **1,** 932 (1968).
[11] J. Haupt, Z. Naturforsch. **26a,** 1578 (1971).
[12] Z. T. Lalowicz, C. A. Mc Dowell, and P. Raghunathan, J. Chem. Phys. **70,** 4819 (1979), erratum ibid. **72,** 3441 (1980).
[13] L.-Y. Hsu and C. E. Nordman, Acta Cryst. C **39,** 690 (1983).
[14] M. Prager, J. Stanislawski, und W. Häusler, J. Chem. Phys. **86,** 2563 (1987).
[15] A. S. Montjoie and W. Müller-Warmuth, Z. Naturforsch. **40a,** 596 (1985).
[16] P. Coppens, L. van Gerven, S. Clough, and A. J. Horsewill, J. Phys.: Solid State Phys. **16,** 567 (1983).